

# Fluxoid quantization effects in superconducting mesoscopic Al multiloop structures

V. BRUYNDONCX, C. STRUNK, V. V. MOSHCHALOV,

C. VAN HAESSENDONCK and Y. BRUYNSERAEDE

*Laboratorium voor Vaste-Stoffysica en Magnetisme, Katholieke Universiteit Leuven,  
Celestijnenlaan 200D, B-3001 Leuven, Belgium*

PACS. 73.23 -b - Mesoscopic systems.

PACS. 74.25.Dw - Superconductivity phase diagrams.

PACS. 74.62 -c - Transition temperature variations.

**Abstract.** - We have studied fluxoid quantization effects in mesoscopic Al samples consisting of a small number of square loops. In short microladders a pronounced substructure of the Little-Parks oscillations (i.e. the oscillations of the critical temperature  $T_c$  as a function of the applied magnetic flux  $\Phi$ ) has been found. These new features in  $T_c(\Phi)$  originate from transitions between different quantum states, each having a specific order parameter profile and flow pattern of the supercurrents. The experimental data are in excellent agreement with the  $T_c(\Phi)$  calculated within the de Gennes-Alexander model for superconducting micronetworks.

In single superconducting loops fluxoid quantization gives rise to a circulating supercurrent when the magnetic flux  $\Phi$  threading the loop differs from  $n\Phi_0$ , where  $n$  is an integer number and  $\Phi_0 = h/2e$  is the superconducting flux quantum. The fluxoid quantum number  $n$  has to be chosen in order to minimize the kinetic energy related to this supercurrent. Consequently, the induced supercurrent and thus the critical temperature  $T_c(\Phi)$  oscillate with a flux period  $\Phi_0$ , as observed for the first time in 1963 by Little and Parks [1].

In micronetworks consisting of several loops fluxoid quantization is required for each closed contour. Infinite lattice geometries have been studied both theoretically and experimentally [2,3]. In addition to the single loop periodicity one observed features related to the long range coherence of the superconducting condensate. In periodic networks cusp-like structures in  $T_c(\Phi)$  arise at rational values  $f=p/q$  of  $\Phi/\Phi_0$  [2], where  $\Phi$  is the flux through an elementary cell and  $p$  and  $q$  are small integers. These *maxima* in  $T_c(\Phi)$  correspond to the formation of a commensurate ‘fluxoid’ superlattice on the underlying geometric pattern.

To our knowledge only single loops and large networks have been investigated experimentally. Although several theoretical studies of “intermediate” structures, containing only a few loops, have been performed [4-7], no experimental verification of the theoretical predictions has been carried out up to now. In this Letter we present the experimental normal/superconducting (N/S) phase boundaries of three particular multiloop geometries: the ‘bola’ (two single loops connected by a wire), the ‘double loop’ and the ‘triple loop’ (the last two patterns are ‘microladders’ containing loops with a common strand) (see Fig. 1). While the bola shows the usual Little-Parks oscillations, we find that the microladders show additional structures in  $T_c(\Phi)$ , reminding the behavior of infinite networks. In contrast to the case of infinite networks, however, cusp-like *minima* in  $T_c(\Phi)$  are found at certain  $\Phi = f\Phi_0$ , which indicate transitions between two distinct superconducting states, having a different fluxoid quantum number. A detailed comparison of our experimental data with theoretical calculations supports, for the first time, an early conjecture of Parks [8] that

nodes in the superconducting order parameter may exist in the middle branch of the double loop.

All samples were prepared in a single run by thermal evaporation of pure Al on an oxidized Si substrate. The patterns were defined by using standard electron beam lithography on a PMMA resist bilayer and subsequent lift-off techniques. The important material parameters are the film thickness  $t=34$  nm, the linewidth  $w=130$  nm, and the sheet resistance  $R = 0.6$   $\Omega$  at 4.2K, corresponding to an elastic mean free path  $l \approx 16$  nm [9]. In the ‘dirty limit’ the Ginzburg-Landau (GL) coherence length  $\xi(T) = \xi(0)(1 - T/T_{c0})^{-1/2} = 0.85 \sqrt{\xi_0 l} (1 - T/T_{c0})^{-1/2}$  and the penetration depth  $\lambda(T) = \lambda(0)(1 - T/T_{c0})^{-1/2} = \lambda_L(0) \left( \frac{\xi_0}{2.66l} \right)^{1/2} (1 - T/T_{c0})^{-1/2}$  [10]. Using the listed values for the BCS coherence length  $\xi_0$  and the London penetration depth at zero temperature  $\lambda_L(0)$  [11] we obtain  $\lambda(0) \approx 130$  nm and  $l(0) \approx 90$  nm. From the measured magnetic field period of the oscillations  $\Delta B = \Phi_0 / a^2 = 1.24$  mT we obtain an effective single loop side length  $a = 1.3$  mm, in good agreement with the average of the inner and the outer loop size [12]. Conventional four-point resistance measurements were performed using a PAR 124A lock-in amplifier. A measuring current of 100 nA rms with a frequency of 27 Hz was used and the magnetic field was applied perpendicular to the sample plane. All electrical leads were shielded by pi filters with a cut-off frequency of 1 MHz in order to avoid spurious effects of radio-frequency interference [13]. The phase boundaries (Fig. 2) have been measured resistively using a feedback technique for stabilizing the temperature at the midpoint of the transition, while slowly sweeping the magnetic field.

Figure 2 shows the measured phase boundaries  $T_c(B)$  (or  $T_c(\Phi)$ , where  $\Phi$  denotes the flux enclosed by one loop) for the three structures. Since the individual loop area is identical for all samples, the  $T_c(\Phi)$  curves have the same overall periodicity. The phase boundary of the bola reveals oscillations, which are very similar to the Little-Parks oscillations of a single loop, while for the other two structures extra cusps are found at intermediate values of  $\Phi$ . At  $\Phi/\Phi_0 = n + 1/2$ ,  $n$  being an integer,

the double loop has local maxima, while in the case of the triple loop local minima are found. Below, we will restrict our analysis to a single  $T_c(B)$  oscillation period. First, however, we consider the background depression of  $T_c(B)$  due to the finite linewidth, since it provides an independent method to determine the coherence length  $\xi(0)$ . The background can be described by applying the formula for  $T_c(B)$  of a thin film in a parallel field [10,14]:

$$T_c(B) = T_{c0} \left[ 1 - \frac{\pi^2}{3} \left( \frac{w \xi(0) B}{\Phi_0} \right)^2 \right] . \quad (1)$$

As long as the linewidth  $w$  is much smaller than the loop size, the total shift of  $T_c$  corresponds to the sum of an oscillatory part, and the monotonic background given by Eq. (1). The background is nearly identical for the three samples, indicating negligible variations in coherence length  $\xi(0)$  and in linewidth  $w$  between different samples.

The N/S phase boundaries can be calculated in the framework of the linearized GL theory. For structures consisting of lines with  $w, t \ll \xi(T), \lambda(T)$ , which is indeed the case for all temperatures used in our experiments, the one-dimensional GL equation has to be solved with the appropriate boundary conditions. The sample geometry influences the shape of the N/S phase boundary mainly via the kinetic energy associated with the supercurrents. At the points where the current paths join one imposes

$$\sum_n \left( i \frac{\partial}{\partial x} + \frac{2\pi}{\Phi_0} A_{//}(x) \right) \Psi_n(x) = 0 . \quad (2)$$

The summation is taken over all strands connected to the junction point. Here,  $x$  is the coordinate defining the position on the strands, and  $A_{//}(x)$  is the component of the vector potential along  $x$ . The boundary condition (Eq. (2)) is often called the generalized first Kirchhoff law, ensuring current conservation [5]. The conventional second Kirchhoff law for voltages in an electrical circuit is now replaced by the requirement of having a single valued order parameter  $\Psi$  when integrating along a closed path:  $\oint \partial \alpha(x) / \partial x dx = 2\pi n$ , where  $\alpha$  is the phase of the complex order

parameter  $\Psi(x) = |\Psi(x)|e^{i\alpha(x)}$  and the integer number  $n$  is called the fluxoid quantum number.

In the simplest approach it is assumed that the modulus of the order parameter is spatially constant (London limit (LL)) [4,15]. A parabolic function  $T(\Phi)$  is obtained for each distribution of fluxoids over the loops  $\{n_i\}$ . In contrast, within the de Gennes-Alexander (dGA) approach  $|\Psi(x)|$  is allowed to vary along the strands [5,16,17]. The system of linear equations obtained from Eq. (2) has nontrivial solutions when its determinant is zero. In both cases, the solution with maximal  $T(\Phi)$  has to be selected as  $T_c(\Phi)$ .

In Fig. 3 and 4 single  $T_c(\Phi)$  periods for the bola (Fig. 3), the double loop (Fig. 4a) and the triple loop (Fig. 4b) are shown. The parabolic background (see Eq. (1)) has been subtracted. The dashed lines are the phase boundaries obtained within the LL, while the solid lines give the results from the dGA approach. The discrepancy between the latter approach and the experimental curve can be substantially reduced by adding the effect of the attached leads to the dGA model. The dashed dotted line in Fig. 3 and 4 gives the result of the dGA calculation where the presence of the leads has been included. The inclusion of the leads reduces the amplitude of the  $T_c$  oscillations and gives a much better agreement for the crossover point  $f$  for the double loop (see Fig. 4a). The values for  $\alpha(0)$  obtained from the fits agree within a few percent with the  $\alpha(0)$  values found independently from the monotonic background of  $T_c(\Phi)$  (see Eq. (1)). As predicted by Fink et al. [5],  $T_c(\Phi)$  of the bola is the same as for a single loop, provided that the length of the strand connecting the two loops (0.2 mm in Fig. 3) is short. In what follows we will focus on the phase boundaries of the double (Fig. 4a) and triple loops (Fig. 4b).

According to the theory, the local cusp-like *minima* in  $T_c(\Phi)$  at  $\Phi = f \Phi_0$  originate from transitions between different quantum states. The value of  $f$  is not a simple ratio of small integers: from the dGA approach we have obtained  $f \approx 0.36$  for the double loop and  $f \approx 0.30$  for the triple loop. This is in contrast to the case of periodic networks, where *maxima* are found at rational  $f$  values  $1/2$ ,  $1/3$ , etc. [2],

which indicate an optimal geometric matching between the fluxoid distribution and the network pattern.

To facilitate the discussion we divide the flux period in two intervals: flux regime I for  $\Phi < f\Phi_0$  or  $\Phi > (1-f)\Phi_0$  and flux regime II for  $f\Phi_0 < \Phi < (1-f)\Phi_0$ . In the flux regime I the theoretical phase boundaries are nearly identical. Near  $\Phi/\Phi_0 = 1/2$  (flux regime II), however, clear differences are found between the dGA approach and the LL. The dGA result fits better to the experimental data with respect to the crossover point  $f$  between regimes I and II, and the amplitude of the  $T_c$  oscillations.

Using the dGA approach we have calculated the spatial modulation of  $|\Psi|$  and the supercurrents for different  $\Phi/\Phi_0$  values at the  $T_c(\Phi)$  boundary. In the flux regime I  $|\Psi|$  varies only slightly and therefore the results of the LL and the dGA models nearly coincide. The elementary loops have an equal fluxoid quantum number (and consequently an equal supercurrent orientation) for both the double and the triple loop geometry. For the double loop this leads to a cancellation of the supercurrent in the middle strand, while for the triple loop structure the fluxoid quantization condition results in a different value for the supercurrent in the inner and the outer loops. As a result, the common strands of the triple loop structure carry a finite current.

In the flux regime II qualitatively different states are obtained from the LL and the dGA approach: the states calculated within the dGA approach have  $|\Psi|$  strongly modulated along the strands. This is most severe for the double loop:  $\Psi$  shows a node ( $|\Psi|=0$ ) in the center of the common strand (the point labeled N in Fig. 4a), the phase  $\alpha$  having a discontinuity of  $\pi$  at this point. This node is a one-dimensional analog of the core of an Abrikosov vortex, where the order parameter also vanishes and the phase shows a discontinuity. In the inset of Fig. 4a the spatial variation of  $|\Psi|$  along the strands is shown for  $\Phi/\Phi_0$  close to the crossover point  $f$ . The solid curve gives  $|\Psi|$  in flux regime I, which is quasi-constant. The strongly modulated solution, which goes through zero in the center, is indicated by the dashed line. Although there exists a finite phase difference across the junction points of the middle strand, no supercurrent can

flow through the strand due to the presence of the node. This node is predicted to persist when moving below the phase boundary into the superconducting state [6,7]. Already in 1964 Parks [8] anticipated that, in a double loop, ‘a part of the middle link will revert to the normal phase’, and that ‘this in effect will convert the double loop to a single loop’, giving an intuitive explanation for the maximum  $T_c(\Phi)$  at  $\Phi/\Phi_0=1/2$ . Such a modulation of  $|\Psi|$  is obviously excluded in the LL, where the loop currents have opposite orientation and add up in the central strand, thus giving rise to a rather high kinetic energy.

For the triple loop structure the modulation of  $|\Psi|$  is still considerable in flux regime II, but it does not show any nodes. Therefore the supercurrent orientations can be found from the fluxoid quantum numbers  $\{n_i\}$ , obtained from integrating the phase gradients along each individual loop. The inset of Fig. 4b shows the fluxoid distribution  $\{n_i\}$  for the different flux regimes. When passing through the crossover point between flux regime I and regime II only the supercurrent in the middle loop is reversed, while increasing the flux above  $\Phi/\Phi_0=1/2$  implies a reversal of the supercurrent in all loops.

Surprisingly, the behavior of a microladder with a linear arrangement of  $m$  loops appears to be qualitatively different for even and for odd  $m$  in the sense that  $m$  determines the presence or absence of nodes in the common strands. For an infinitely long microladder  $|\Psi|$  was found to be spatially constant below a certain  $\Phi < \Phi_c$  [18], which is analogous to the states we find in flux regime I. For fluxes  $\Phi > \Phi_c$  modulated  $|\Psi|$  states, with an incommensurate fluxoid pattern, were found. At  $\Phi/\Phi_0=1/2$ , nodes appear at the center of every second common (transverse) branch.

In conclusion, we have shown that mesoscopic microladders exhibit new features in the phase boundary  $T_c(\Phi)$  when compared to the classical Little-Parks effect. These additional features arise from transitions between quantum states with weakly and strongly modulated order parameter  $|\Psi|$ . Moreover, the fluxoid distribution, and therefore also the supercurrent flow along the loops, is qualitatively different for these states. The phase boundaries were calculated within the London limit, as well as within the de Gennes-Alexander approach. The latter gives the better

quantitative agreement with our experimental results, certainly when the effect of the attached leads is incorporated into the model.

\*\*\*

The authors wish to thank T. Puig, E. Rosseel and A. López for fruitful discussions, M. Van Bael for the AFM pictures and R. Jonckheere for the lithography. We are grateful to the Belgian National Fund for Scientific Research (NFWO), the Flemish Concerted Action (GOA), the Belgian Inter-University Attraction Poles (IUAP) and the European Human Capital and Mobility (HCM) research programs for the financial support.

#### REFERENCES

- [1] W. A. LITTLE and R. D. PARKS, Phys. Rev. Lett. **9**, 9 (1962); R. D. PARKS and W. A. LITTLE, Phys. Rev. **133**, A97 (1964).
- [2] B. PANNETIER, J. CHAUSSY and R. RAMMAL, J. Phys. Lett. **44**, L853 (1983); B. PANNETIER *et al.*, Phys. Rev. Lett. **53**, 1845 (1984).
- [3] A. BEHROOZ *et al.*, Phys. Rev. **B35**, 8396 (1987); F. NORI and Q. NIU, Physica B **152**, 105 (1988); J. M. GORDON *et al.*, Phys. Rev. Lett. **56**, 2280 (1986); J. M. GORDON, A. GOLDMAN and B. WHITEHEAD, Phys. Rev. Lett. **59**, 2311 (1987).
- [4] C. C. CHI, P. SANTHANAM and P. E. BLÖCHL, J. Low Temp. Phys. **88**, 163 (1992).
- [5] H. J. FINK, A. LÓPEZ and R. MAYNARD, Phys. Rev. **B26**, 5237 (1982).
- [6] C. AMMANN, P. ERDÖS and S. B. HALEY, Phys. Rev. **B51**, 11739 (1995).
- [7] J. I. CASTRO and A. LÓPEZ, Phys. Rev. **B52**, 7495 (1995).
- [8] R. D. PARKS, Science **146**, 1429 (1964).

- [9] J. ROMIJN *et al.*, Phys. Rev. **B26**, 3648 (1982).
- [10] M. TINKHAM, Phys. Rev. **129**, 2413 (1963) and in: *Introduction to Superconductivity* (McGraw-Hill, New York, 1975).
- [11] P. G. DE GENNES, *Superconductivity of Metals and Alloys* (Benjamin, New York, 1966).
- [12] R. P. GROFF and R. D. PARKS, Phys. Rev. **176**, 567 (1968).
- [13] C. STRUNK *et al.*, Phys. Rev. **B53**, 11332 (1996).
- [14] V. V. MOSHCHALOV *et al.*, Nature **373**, 319 (1995).
- [15] S. ALEXANDER and E. HALEVI, J. Phys. (Paris) **44**, 805 (1983).
- [16] P. G. DE GENNES, C. R. Acad, Sci. Ser. **II 292**, 279 (1981).
- [17] S. ALEXANDER, Phys. Rev. **B27**, 2820 (1983).
- [18] J. SIMONIN, D. RODRIGUES and A. LÓPEZ, Phys. Rev. Lett. **49**, 944 (1982).

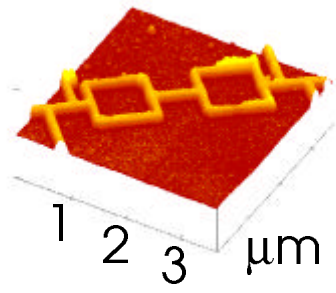
## FIGURE CAPTIONS

Fig. 1 AFM micrographs of the studied structures: a) the bola, b) the double loop, and c) the triple loop structure.

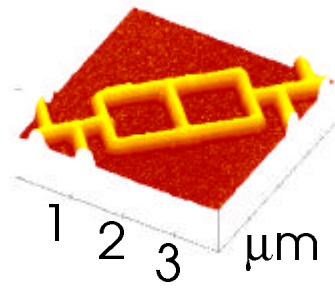
Fig. 2 Experimental N/S phase boundaries  $T_c(\Phi)$ . For the bola  $T_c(\Phi)$  is very similar to the Little-Parks  $T_c(\Phi)$  of a single loop, while the other two samples show additional features. The curves have been shifted along the x-axis for clarity.

Fig. 3 Detail of Fig. 2 (one single period) for the bola. The dots are the experimental datapoints with the parabolic background subtracted, while the lines correspond to the different theoretical results as explained in the text. The value for  $\chi(0)$  shown on the graph is determined by fitting the experimental data to the theory.

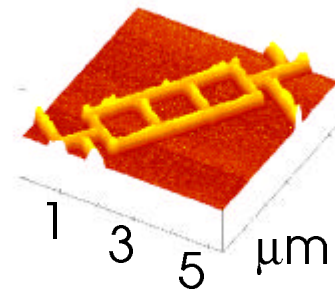
Fig. 4 Detail of Fig. 2 (one single period) for (a) the double loop and (b) the triple loop. The dots are the experimental datapoints with the parabolic background subtracted, while the lines correspond to the different theoretical results as explained in the text. The values for  $\chi(0)$  shown on the graphs are determined by fitting the experimental data to the theory. The insets in (a) shows the calculated variation of  $|\Psi|$  along the strands. The solid line is the nearly constant  $|\Psi|$  solution, while the dashed line is the state with a node in the center point N. The inset in (b) gives the fluxoid distribution in the different flux regimes for the triple loop.



**(a) Bola**



**(b) Double Loop**



**(c) Triple Loop**

